Coarsening Behavior of Bulk Nanobubbles in Water

Jeong Il Lee
Chung-Ang University
Han Sol Huh
Chung-Ang University
Joong Yull Park
Chung-Ang University
Jung-Geun Han (jghan@cau.ac.kr)
Chung-Ang University
Jong-Min Kim
Chung-Ang University

Research Article

Keywords: Nanofluidic, Nanobubble, Carbon dioxide gas, Particle coarsening, Nanoparticle tracking analysis

Posted Date: June 18th, 2021

DOI: https://doi.org/10.21203/rs.3.rs-620470/v1

Coarsening behavior of bulk nanobubbles in water

Jeong Il Lee[1], Han Sol Huh[1], Joong Yull Park[1], Jung-Geun Han[2,3,*], and Jong-Min Kim[1,**]

[1]School of Mechanical Engineering, Chung-Ang University, Seoul 06974, Republic of Korea

[2]School of Civil and Environmental Engineering, Chung-Ang University, Seoul 06974, Republic of Korea

[3]Department of Intelligent Energy and Industry, Chung-Ang University, Seoul 06974, Republic of Korea

ABSTRACT

In recent years, extremely small gas bubbles called bulk nanobubbles (BNBs) have drawn great attention due to their impressive effects and their wide applicability in a variety of technological fields, including biomedical engineering, water treatment, and nanomaterials. However, unsolved questions remain regarding the stability and behavior of BNBs. In the present work, BNBs were generated in water using a gas-liquid mixing method. To investigate the coarsening behavior of BNBs in water over time, particle analysis was performed using a nanoparticle tracking analysis (NTA) method. Over time, the BNB diameter continuously increased (from 88.50 nm to 201.00 nm), and its cubic radius increased linearly ($r^3 \sim t$). While the concentration of BNBs decreased (from 3.47 $\times 10^8$ particles/mL to 0.61 $\times 10^8$ particles/mL), the total volume of BNBs remained the same. Moreover, the size distribution broadened over time, and the concentration of larger BNBs gradually increased over time. These results indicate that relatively small BNBs disappear and larger BNBs grow through mass transfer between BNBs instead of dissolution of the gas and coalescence. In other words, BNBs underwent Oswald

ripening; that is, gas molecules detached from smaller BNBs, diffused into the continuous phase, and then were absorbed into larger BNBs.

Keywords:

Nanofluidic; Nanobubble; Carbon dioxide gas; Particle coarsening; Nanoparticle tracking analysis

* Corresponding author

Jung-Geun Han, E-mail: jghan@cau.ac.kr

** Corresponding author

Jong-Min Kim, E-mail: 0326kjm@cau.ac.kr

1. Introduction

In recent years, many researchers have been interested in bulk nanobubbles (BNBs) because of their impressive characteristics, including long lifespan[1], acceleration of metabolism[2], improvement in fossil fuel combustion[3-4], cleaning ability[5-6], and utility as a contrast agent and in drug delivery[7]. However, unsolved questions remain regarding the stability of BNBs and the principles of their application. According to the Young–Laplace equation, the internal pressure within BNBs is much greater than atmospheric pressure. Consequently, BNBs are not stable under atmospheric conditions. Ohgaki et al.[8] reported that the internal pressure of BNBs is about twice as large as that calculated using the Young–Laplace equation. They fabricated BNBs of three different gases (N_2, CH_4, and Ar) and showed that their internal pressures were 5.6–6.3 MPa for a 50 nm radius each NB, whereas the corresponding internal pressure

predicted by the Young–Laplace equation was about 2.9 MPa. In contrast, the internal pressure of the BNBs has also been reported to be lower than that calculated using the Young–Laplace equation. Nagayama et al.[9] showed that there are few vapor atoms in the nanobubbles using molecular dynamics simulation. They concluded that the internal pressure of a nanobubble is much lower than that estimated by the Young–Laplace equation because nanobubbles have few atoms.

In the fields of biological and medical research, BNBs are potential materials for cell culture, targeted drug delivery and ultrasound imaging. Ebina et al.[2] reported that oxygen and air BNBs could potentially be effective tools for growing living things. The authors experimentally showed the accelerated growth of various living things such as Brassica campestris, sweetfish, rainbow trout and DBA1/J mice using BNBs. BNBs are also used as contrast agents, and it is known that the acoustic response of contrast agents is directly related to the particle size of the agent. Several researchers have demonstrated the potential for improving ultrasound contrast sensitivity by changing the size and size distribution of the BNBs used[10-14]. Talu et al.[10] demonstrated that the pulse shapes of echoes from groups of uniformly sized bubbles are almost the same, while those of polydisperse bubbles are not. They also stated that optimization of the size distribution of contrast agents has the potential to enhance the sensitivity of contrast imaging. However, such a system could be influenced by ambient conditions, and variations in ambient conditions after injection into the incubating system or body may change the size distribution and concentration of BNBs. To fully exploit these potential possibilities, a thorough understanding of the behavior of BNBs is needed.

In this study, we examined the coarsening behavior of BNBs in water over time. BNBs were generated by using carbon dioxide (CO_2) gas and distilled (DI) water through gas-liquid mixing method[15]. Also, the presence of fabricated BNBs were investigated using attenuated total

reflectance Fourier transform infrared (ATR-FTIR) spectroscopy and their size distribution and concentration were investigated over time by using a nanoparticle tracking analysis (NTA) method. It is demonstrated that the BNBs grow over time by diffusing from smaller to larger BNBs (Ostwald ripening phenomenon).

2. Experimental setup

Materials. Carbon dioxide (CO_2) gas (purity: 99.9 %, Shinyoung Gas Co., Republic of Korea), which can be identified using infrared spectroscopy, and distilled (DI) water (No. 119, HPLC grade, Duksan Pure Chemicals Co., Republic of Korea) were used to fabricate BNB water. Also, a vial 4 mL in volume (SL.Vi1151, SciLab Korea Co., Ltd., Republic of Korea) and its screw cap (SL.Vi1164, SciLab Korea Co., Ltd.) were prepared. These materials were used as received except for the vial and screw cap. Before BNB fabrication, the vial and its cap were cleaned using DI water to eliminate the dust from the vial, cap and septa.

Generation of bulk nanobubbles. In this study, a gas-liquid mixing (agitation) method[15] was used to generate a large number BNBs in water. A nanobubble generator, which consists of a vial holder and a linear actuator, was used to generate the BNBs. The actuator was driven by an electric motor, and rotational motion generated by the motor was converted into linear motion by a crank. Then, the linear motion was transmitted using a connecting rod to the vial holder. Thus, the vial holder moved up-and-down to mix the CO_2 gas and water in the vial. The following settings were used to generate the BNBs in water: the motor velocity was 90 rpm, the stroke was 20 cm, the gas-liquid ratio was 1:1, and the mixing time was 2 hours.

Nanobubble analysis. For the NB analysis in water, a nanoparticle tracking analysis (NTA) method was used by using a NTA instrumnet with a blue polarized 405 nm laser (NanoSight

LM10-HSBFT14, Quantum Design Korea, Republic of Korea). It is a NB visualization technique that provides size, count, and concentration measurements. As the laser light illuminates the NBs, the Brownian motion of NBs is detected and the light scattering properties of the NBs is detected. The NBs could be visualized directly in water and captured using a CCD camera to obtain the bubble size distribution, which consists of bubble diameter and concentration. The NB concentration is the total number of NBs, 10−1000 nm in diameter, per milliliter. Each measurement was recorded more than five times.

Fourier Transform Infrared Spectroscopy. There are many gases (CO_2, CO, CH_4 and so on) that are infrared (IR) active. However, CO_2 gas is particularly suited for IR techniques because gaseous CO_2 and dissolved CO_2 show different IR spectra. In this study, an attenuated total reflectance Fourier transform infrared (ATR-FTIR) spectrometer (Thermo Nicolet 6700, Scinco Co., Ltd., Republic of Korea) equipped with a liquid nitrogen cooled mercury-cadmium-telluride (MCT) detector was used to investigate the nature of the gas in the fabricated BNBs. The infrared spectra were recorded with a resolution of 0.5 cm^{-1} and a total of 200 scans were measured in the range of 650−4000 cm^{-1} at ambient conditions.

3. Results and discussion

Generation of bulk nanobubbles. BNBs were successfully fabricated with CO_2 gas in DI water using a BNB generator with a linear actuator. We captured images of the BNBs successfully using CCD camera and measured the size distribution just after BNB generation (Figure 1). Laser-illuminated BNBs are represented as bright white dots in Fig. 1a, and larger BNBs are brighter than small ones. As shown in Fig. 1b, the size distribution of the BNBs has a single peak. The mean and mode diameters of the BNBs were 88.80 ± 9.59 nm and 70.63 ±

9.47 nm, respectively, and the concentration of the BNBs was 3.47 ± 0.39 × 10^8 particles/mL. Prior to BNB generation, no nano-sized particles were detected in the DI water. Based on these results, we concluded that BNBs were successfully generated by mixing CO_2 gas and DI water together.

The existence and stability of BNBs has been discussed with regard to the high internal pressure of the BNBs. According to the Young–Laplace equation (Eq. 1), the pressure difference between the inside and outside of a bubble is inversely proportional to the diameter of bubble:

$$P_{in} - P_{amb} = \frac{4\sigma}{d} \tag{1}$$

Here, P_{in}, P_{amb}, σ, and d are the internal pressure of the BNB, the ambient pressure, the surface tension of the liquid, and the diameter of the bubble, respectively. In this study, the internal pressure of the BNB would be approximately 3.40 MPa according to this equation (using d = 88.50 nm and σ = 0.073 N/m). Therefore, BNBs should be stable at ambient conditions due to this high internal pressure, and they should collapse very quickly.

Moreover, according to a study performed by Ljunggren et al.[16], the lifetime of a bubble is described as:

$$t = \frac{Kd_0^{\,2}}{12RTD}, \tag{2}$$

Here, K, d_0, R, T and D are Henry's law constants, the bubble diameter at t = 0, the gas constant, temperature, and the diffusion constant, respectively. Thus, the lifetime of a BNB used in this study would be approximately 0.49 μs (using K = 2.98 ×10^3 J/mol, d_0 = 88.50 nm, R = 8.314 J/(K·mol), T = 298.15 K, and D = 1.60 × 10^{-9} m^2/s).

However, recent experimental studies showed that BNBs exist stably under atmospheric pressure, and their lifespan exceeds analytic expectations[17-18]. In addition, other investigators revealed that the interface of BNBs consists of hard hydrogen bonds that are similar to hydrogen bonds found in ice and gas hydrates[8, 19-20]. Thus, it is believed that the hard interface leads to reduced diffusivity of gas molecules in the BNB and a high surface tension, which helps to maintain an adequate kinetic balance of BNBs against high internal pressure.

Meanwhile, ATR-FTIR spectroscopy was used for the detection of BNBs created from CO_2 gas, and ATR-FTIR spectra of the fabricated BNBs were recorded. The ATR-FTIR spectra of gaseous CO_2 in BNBs is shown in Fig. 2, and the result clearly shows two branches with fine lines at about 2300 to 2380 cm^{-1} (represented as a black solid line shown in Fig. 2). The resulting IR spectrum represents the molecular absorption and transmission because the molecule absorbs particular frequencies that are characteristic of its structure. This means that a sample has a molecular fingerprint, and no two molecular structures create the same IR spectrum. This makes IR spectroscopy useful for several types of analysis. Because gaseous and dissolved CO_2 gas exhibit very different IR spectra[21], IR spectroscopy can be used to directly identify the phase state of the CO_2 molecules. Lohse et al.[21] showed that the IR spectrum of gaseous CO_2 consists of two branches with fine lines at 2300 to 2380 cm^{-1}, while that of dissolved CO_2 in water shows a single peak at about 2340 cm^{-1}. Similarly, Zhang et al.[22] experimentally demonstrated that a very thin gas domain (i.e., surface nanobubble) consists of gaseous CO_2, and their lifespan was longer than 1 h. These authors performed ATR-FTIR spectroscopy and showed that the ATR-FTIR spectrum measured from surface nanobubbles is the same as that of CO_2 gas (represented as gray solid lines shown in Fig. 2). The obtained ATR-FTIR spectrum of BNBs showed the same shape and band position (represented as a black solid line) as the standard gaseous CO_2 spectrum. This result reveals that the fabricated BNBs

in this study were filled with CO_2 gas.

Coarsening of bulk nanobubbles. To observe the coarsening behavior of BNBs, fabricated BNB water was placed in a room for 6 d and particle analysis was performed. Images of BNBs in water taken over time showed that the number of BNBs (seen as white bright circles on the dark background of the water in Fig. 3) decreased with time. The mean and mode diameter of BNBs were initially 88.50 ± 9.59 nm and 70.63 ± 9.47 nm, respectively, and the BNB concentration was 3.47 ± 0.39 $\times 10^8$ NBs/mL (Fig. 4).

The mean and mode diameter of the BNBs started to increase during the aging test. In contrast, the concentration of BNBs decreased with time, and it took 2 days to reach half of the initial concentration. After 6 d of aging, the mean and mode diameters were 201.00 ± 12.12 nm and 166.33 ± 39.70 nm, respectively, and the concentration was 0.61 ± 0.03 × 10^8 NBs/mL. In short, the growth of BNBs showed a continuous increase in diameter, and the measured diameters did not indicate a jump in BNB diameter, which can occur after a coalescence event.

Moreover, during the aging test, the total volume of BNBs was almost unchanged (Fig. 4(b)). To evaluate the time effect on the total volume of BNBs, one-way analysis of variance (ANOVA) was performed, and the P-value was calculated to be 0.08, which is much larger than the significance level (0.05). This means that the change in total volume is negligible within about 6 d. Therefore, it is reasonable to assume that most of the fabricated BNBs did not dissolve during the aging test, and changes in diameter and concentration are largely based on mass transfer between BNBs.

The time for growth of bubbles in an oversaturated solution can be calculated based on Epstein-Plesset theory[23]:

$$\varepsilon^2 = 1 + x^2 , \tag{3}$$

$$\varepsilon = \frac{r}{r_0}, \tag{4}$$

$$x^2 = \frac{2\alpha}{r_0^{\,2}} t, \tag{5}$$

$$\alpha = \frac{D\left(c_i - c_s\right)}{\rho}, \tag{6}$$

where ε is the ratio of the bubble radius to its initial radius, and x is a dimensionless variable proportional to the square root of the time. R and r_0 (at initial time) are radii of gas bubble. α is positive constant and t is time. D, c_i, c_s, and ρ are the coefficient of diffusivity of the gas in the liquid, initial dissolved gas concentration, concentration at saturation, and gas density, respectively. According to Eqs. (3−6), if the BNB water used in this study was slightly oversaturated with CO_2 (i.e. $c_i/c_s \approx 1$, but > 1), BNBs that were initially 88.50 nm in mean diameter would grow to 201.00 nm in a very short time. The order of magnitude of the time required for bubble growth is approximately -20 (using $D = 1.60 \times 10^{-9}$ m^2/s and $\rho = 1.81$ kg/m^3). This result suggests that there is something that hinders gas diffusion at the gas-liquid interface.

To investigate the obtained BNB changes in further detail, the time evolution of BNB size distribution was examined. The time evolution of size distribution data (Fig. 5(a)) show that BNBs initially had a right-skewed size distribution. Also, there were few BNBs larger than 200 nm in diameter just after fabrication. However, after 1 d, the shape of the size distribution changed to show a multi-peak distribution, and BNBs larger than 200 nm were apparent (Fig. 5(a)). In the later stages, the size distribution became broader because of the presence of larger BNBs, which were not detected in the early stages (Figs. 5(b−d)). Taken as a whole, the number of BNBs decreased and their size distribution broadened with time; that is to say, relatively large bubbles tended to appear and relatively small bubbles tended to disappear over 6 d.

This result suggests that a thermodynamically driven spontaneous process occurred in the BNB water system. Generally, larger particles are more energetically stable than smaller particles. As the system moves toward a lower overall energy, molecules on the surface of a smaller particle tend to detach and diffuse through the solution. Diffused molecules then attach to the surface of larger particles and are absorbed into them. Therefore, the number of smaller particles decreases, while larger particles grow in size[24]. There was a large number of relatively larger BNBs in the early stages of the aging test, most of which ranged in diameter from 150 nm to 250 nm. Thus, gas molecules that detached from small BNBs could easily attach to the surfaces of the BNBs of this size, thereby increasing their concentration further. Because the peak of the size distribution moved to the right over time (Fig. 5), we would expect the concentration of BNBs over 600 nm in diameter to increase if aging were allowed to continue.

However, there are two main particle coarsening pathways in nanoscale systems: Ostwald ripening and Smoluchowski ripening. The former is the process by which larger particles grow while smaller particles shrink. Molecules detached from smaller particles diffuse over the continuous phase until they join larger nanoparticles. Moreover, this particle coarsening process can occur even in a microscale gas-liquid system. Talu et al.[25] showed that Ostwald ripening can occur even if the microbubbles are initially monodispered. In contrast, Smoluchowski ripening is caused by collisions between nanoparticles as they move throughout the continuous phase. Brownian motion is the random movement of particles in fluids. BNBs suspended in water also tend to move at random. These motions can cause the BNBs to collide with each other, leading to coalescence and coarsening of bubbles, thereby increasing the mean diameter of BNBs and decreasing the number of BNBs. To prevent the BNBs from colliding and coalescing, the BNBs should repel each other. Along these lines, it has been reported that BNBs are supported by electrically charged liquid–gas interfaces, which create repulsive forces

that prevent BNBs from colliding and coalescing[19, 26]. Also, if the concentration of BNBs is low enough, their chance of colliding becomes low[27]. Assuming that the BNBs were well dispersed in water, the distance between neighboring BNBs fabricated in this study would have been about 14.23 μm just after fabrication, or about 322 times the mean radius of the BNBs. Thus, collisions between BNBs would be infrequent in the BNB water used in this study, and therefore Ostwald ripening likely dominated the particle coarsening. Moreover, the BNB diameter data over time presented in Fig. 4(a) did not show jumps in BNB sizes that would correspond to a coalescence event.

Ostwald ripening is a direct consequence of the Kelvin effect[28-29]. The solubility of the particle increases dramatically as its size decreases according to the Kelvin equation:

$$S(r) = S(\infty)\exp\left(\frac{2\gamma V_m}{rRT}\right), \tag{7}$$

Here, S(r) is the solubility of the medium surrounding a particle of radius r, S(∞) is the bulk solubility, γ is the interfacial tension, V_m is the molar volume of the dispersed phase, R is the gas constant, and T is the absolute temperature. Based on the Kelvin equation, smaller particles are more soluble than larger particles. The smaller particles tend to lose their molecules, which diffuse through the continuous phase and are absorbed by larger particles. Thus, relatively small particles become smaller, while larger particles grow. Consequently, the number of smaller particles decreases and that of larger particles increases. This prediction agrees well with the tendency shown in Figs. 4 and 5.

In many studies, researchers have tried to establish a connection between the particle size distribution and the coarsening mechanism[30-34]. In these studies, the shape of the size distribution was considered as a criterion for classifying the coarsening mechanism. Granqvist et al.[32] reported that size distributions that lean toward the smaller particle sizes (i.e., left-

skewed size distributions) and have a sharp cutoff above a certain size are characteristic of the Ostwald ripening process. In contrast, right-skewed size distributions (i.e., those that lean toward larger particle sizes, or are log-normal) have been attributed to Smoluchowski ripening.

In our system, although the number of BNBs tended to decrease and their size distribution broadened with time, the time evolution of the BNB size distribution showed right-skewed size distributions (Fig. 5). Despite the right-skewed distributions of particles, Ostwald ripening is dominant during the particle coarsening process[33-35]. Datye et al.[34] showed that the shape of the particle size distribution cannot be used as a criterion for determining the dominant coarsening mechanism, especially when Ostwald ripening and Smoluchowski ripening may happen concurrently. In addition, De Smet et al.[36] experimentally demonstrated that the droplet size distribution in a stabilized emulsion of tetradecane in water was symmetrical, which was quite different from the size distribution predicted by the Lifshitz–Slyozov–Wagner (LSW) theory.

The time evolution of the cubic BNB radius r^3 is presented in Fig. 6. In the aging test, the measured cubic radius increased linearly with time, and the slope of the fit line was about 1.45 $\times 10^5$ nm^3/d. In other words, the cubic radius resembles the trend predicted by the LSW theory for Ostwald ripening; that is, the mean particle radius, r is proportional to time, t (i.e., $r^3 \sim t$)[37-38]. This observation could be caused by the following reasons: (1) collision of neighboring BNBs does not occur due to the low concentration of BNBs and a negatively charged bubble surface, and (2) LSW theory explicitly omits particle aggregation[39]. Therefore, these results indicate that BNBs underwent Oswald ripening and relatively small BNBs disappear and larger BNBs grow through mass transfer between BNBs instead of dissolution of the gas and coalescence.

4. Conclusions

In the present study, BNB water was prepared using a gas-liquid mixing method, and its particle coarsening mechanism was investigated using an NTA method. BNBs were successfully fabricated with CO_2 gas in DI water by using a BNB generator with a linear actuator, and the ATR-FTIR spectra of BNBs showed two branches with fine lines at 2300 to 2380 cm^{-1}, which reveal that the BNBs were filled with CO_2 gas. During the 6 d of the aging test, the growth of BNBs showed a continuous increase in diameter, and measured diameters showed that there were no jumps in BNB diameter as would be expected after a coalescence event. Even though the concentration of BNBs decreased with time, the total volume of BNBs remained unchanged. These results indicate that most of the fabricated BNBs did not dissolve, but mass transfer between BNBs did occur. In addition, BNBs had a right-skewed size distribution, and the size distribution of the BNBs initially showed a single-peak distribution, but after aging the size distributions included two or three peaks of larger diameters. At the same time, the peak in the size distribution moved right over time. This means that the relatively small bubbles decreased in number, and relatively large bubbles increased in size over time. Moreover, the time evolution of the cubic BNB radius r^3 increased linearly with time, and this cubic radius resembled the trend predicted by the LSW theory for Ostwald ripening (i.e., $r^3 \sim t$). This is because: (1) the chance of BNB collision is very low due to the low concentration of BNBs and negatively charged bubble surfaces, and (2) LSW theory explicitly omits particle aggregation. We believe that this study provides the important information to understand the exact mechanism of the coarsening behavior of BNBs in the NB solutions especially for biomedical applications.

Acknowledgements

This work has supported by the National Research Foundation of Korea(NRF) grant funded by the Korea government(MSIT)(No. 2017R1A2B4007923).

References

1. Ulatowski, K.; Sobieszuk, P.; Mróz, A.; Ciach, T., Stability of nanobubbles generated in water using porous membrane system. *Chemical Engineering and Processing-Process Intensification* **2019,** *136*, 62-71.

2. Ebina, K.; Shi, K.; Hirao, M.; Hashimoto, J.; Kawato, Y.; Kaneshiro, S.; Morimoto, T.; Koizumi, K.; Yoshikawa, H., Oxygen and air nanobubble water solution promote the growth of plants, fishes, and mice. *PLoS One* **2013,** *8* (6), e65339.

3. Oh, S. H.; Yoon, S. H.; Song, H.; Han, J. G.; Kim, J.-M., Effect of hydrogen nanobubble addition on combustion characteristics of gasoline engine. *Int J Hydrogen Energ* **2013,** *38* (34), 14849-14853.

4. Nakatake, Y.; Kisu, S.; Shigyo, K.; Eguchi, T.; Watanabe, T., Effect of nano air-bubbles mixed into gas oil on common-rail diesel engine. *Energy* **2013,** *59*, 233-239.

5. Zhu, J.; An, H.; Alheshibri, M.; Liu, L.; Terpstra, P. M.; Liu, G.; Craig, V. S., Cleaning with bulk nanobubbles. *Langmuir* **2016,** *32* (43), 11203-11211.

6. Zhang, M.; Seddon, J. R., Nanobubble–nanoparticle interactions in bulk solutions. *Langmuir* **2016,** *32* (43), 11280-11286.

7. Wang, C.-H.; Huang, Y.-F.; Yeh, C.-K., Aptamer-conjugated nanobubbles for targeted ultrasound molecular imaging. *Langmuir* **2011,** *27* (11), 6971-6976.

8. Ohgaki, K.; Khanh, N. Q.; Joden, Y.; Tsuji, A.; Nakagawa, T., Physicochemical approach to

nanobubble solutions. *Chem Eng Sci* **2010,** *65* (3), 1296-1300.

9. Nagayama, G.; Tsuruta, T.; Cheng, P., Molecular dynamics simulation on bubble formation in a nanochannel. *Int J Heat Mass Tran* **2006,** *49* (23-24), 4437-4443.

10. Talu, E.; Hettiarachchi, K.; Zhao, S.; Powell, R. L.; Lee, A. P.; Longo, M. L.; Dayton, P. A., Tailoring the size distribution of ultrasound contrast agents: possible method for improving sensitivity in molecular imaging. *Molecular imaging* **2007,** *6* (6), 7290.2007. 00034.

11. Sirsi, S.; Feshitan, J.; Borden, M.; Homma, S. In *High-frequency ultrasound imaging of size-isolated microbubbles in mice*, 2009 IEEE International Ultrasonics Symposium, IEEE: 2009; pp 271-274.

12. Kaya, M.; Feingold, S.; Streeter, J.; Hettiarachchi, K.; Lee, A. P.; Dayton, P. A. In *Acoustic characterization of individual monodisperse contrast agents with an optical-acoustical system*, 2009 IEEE International Ultrasonics Symposium, IEEE: 2009; pp 1813-1816.

13. Streeter, J. E.; Gessner, R.; Miles, I.; Dayton, P. A., Improving sensitivity in ultrasound molecular imaging by tailoring contrast agent size distribution: in vivo studies. *Molecular imaging* **2010,** *9* (2), 7290.2010. 00005.

14. Wang, Y.; Li, X.; Zhou, Y.; Huang, P.; Xu, Y., Preparation of nanobubbles for ultrasound imaging and intracelluar drug delivery. *Int J Pharmaceut* **2010,** *384* (1-2), 148-153.

15. Oh, S. H.; Kim, J.-M., Generation and stability of bulk nanobubbles. *Langmuir* **2017,** *33* (15), 3818-3823.

16. Ljunggren, S.; Eriksson, J. C., The lifetime of a colloid-sized gas bubble in water and the cause of the hydrophobic attraction. *Colloids and Surfaces A: Physicochemical and Engineering Aspects* **1997,** *129*, 151-155.

17. Michailidi, E. D.; Bomis, G.; Varoutoglou, A.; Kyzas, G. Z.; Mitrikas, G.; Mitropoulos, A. C.; Efthimiadou, E. K.; Favvas, E. P., Bulk nanobubbles: Production and investigation of their formation/stability mechanism. *J Colloid Interf Sci* **2020,** *564*, 371-380.

18. Nirmalkar, N.; Pacek, A.; Barigou, M., On the existence and stability of bulk nanobubbles. *Langmuir* **2018,** *34* (37), 10964-10973.

19. Takahashi, M., Base and technological application of micro-bubble and nanobubble. *Materials Integration* **2009,** *22* (5), 2-19.

20. Nakashima, S.; Spiers, C.; Mercury, L.; Fenter, P.; Hochella Jr, M., Physicochemistry of Water in Geological and Biological Systems.

21. Lohse, D.; Zhang, X., Surface nanobubbles and nanodroplets. *Reviews of modern physics* **2015,** *87* (3), 981.

22. Zhang, X. H.; Khan, A.; Ducker, W. A., A nanoscale gas state. *Phys Rev Lett* **2007,** *98* (13), 136101.

23. Epstein, P. S.; Plesset, M. S., On the stability of gas bubbles in liquid-gas solutions. *The Journal of Chemical Physics* **1950,** *18* (11), 1505-1509.

24. Ratke, L.; Voorhees, P. W., Nucleation, growth and coarsening. In *Growth and Coarsening*, Springer: 2002; pp 205-224.

25. Talu, E.; Hettiarachchi, K.; Powell, R. L.; Lee, A. P.; Dayton, P. A.; Longo, M. L., Maintaining monodispersity in a microbubble population formed by flow-focusing. *Langmuir* **2008,** *24* (5), 1745-1749.

26. Cho, S.-H.; Kim, J.-Y.; Chun, J.-H.; Kim, J.-D., Ultrasonic formation of nanobubbles and their zeta-potentials in aqueous electrolyte and surfactant solutions. *Colloids and Surfaces A: Physicochemical and Engineering Aspects* **2005,** *269* (1-3), 28-34.

27. Weijs, J. H.; Seddon, J. R.; Lohse, D., Diffusive shielding stabilizes bulk nanobubble clusters. *ChemPhysChem* **2012,** *13* (8), 2197-2204.

28. Finsy, R., On the critical radius in Ostwald ripening. *Langmuir* **2004,** *20* (7), 2975-2976.

29. Adamson, A. W.; Gast, A. P., *Physical chemistry of surfaces*. Interscience publishers New York: 1967; Vol. 15.

30. Parker, S. C.; Campbell, C. T., Kinetic model for sintering of supported metal particles with improved size-dependent energetics and applications to Au on TiO 2 (110). *Phys Rev B* **2007,** *75* (3), 035430.

31. Jak, M.; Konstapel, C.; Van Kreuningen, A.; Verhoeven, J.; Frenken, J., Scanning tunnelling microscopy study of the growth of small palladium particles on TiO2 (110). *Surface science* **2000,** *457* (3), 295-310.

32. Granqvist, C.; Buhrman, R., Size distributions for supported metal catalysts: Coalescence growth versus ostwald ripening. *Journal of Catalysis* **1976,** *42* (3), 477-479.

33. McCarty, J.; Malukhin, G.; Poojary, D.; Datye, A.; Xu, Q., Thermal coarsening of supported palladium combustion catalysts. *The Journal of Physical Chemistry B* **2005,** *109* (6), 2387-2391.

34. Datye, A. K.; Xu, Q.; Kharas, K. C.; McCarty, J. M., Particle size distributions in heterogeneous catalysts: What do they tell us about the sintering mechanism? *Catalysis today* **2006,** *111* (1-2), 59-67.

35. Goeke, R. S.; Datye, A. K., Model oxide supports for studies of catalyst sintering at elevated temperatures. *Topics in Catalysis* **2007,** *46* (1-2), 3-9.

36. De Smet, Y.; Danino, D.; Deriemaeker, L.; Talmon, Y.; Finsy, R., Ostwald ripening in the transient regime: a cryo-TEM study. *Langmuir* **2000,** *16* (3), 961-967.

37. Zheng, H.; Smith, R. K.; Jun, Y.-w.; Kisielowski, C.; Dahmen, U.; Alivisatos, A. P., Observation of single colloidal platinum nanocrystal growth trajectories. *science* **2009,** *324* (5932), 1309-1312.

38. Murray, C. B.; Kagan, a. C.; Bawendi, M., Synthesis and characterization of monodisperse nanocrystals and close-packed nanocrystal assemblies. *Annual review of materials science* **2000,** *30* (1), 545-610.

39. Lifshitz, I. M.; Slyozov, V. V., The kinetics of precipitation from supersaturated solid

solutions. *Journal of physics and chemistry of solids* **1961,** *19* (1-2), 35-50.

List of Figures

Figure 1. Fabricated BNBs in water. (a) images of BNBs. Black background and white dots represent the water and BNBs, respectively. (b) size distribution of BNBs just after their generation in water.

Figure 2. ATR-FTIR spectra of gaseous CO2 in surface nanobubbles and BNBs. The spectrum shows two groups of distinctive fine peaks that were attributed to CO2 gas molecules. The spectrum of BNB water demonstrates the formation of gaseous CO2 bubbles.

Figure 3. Images of BNBs in water: (a) just after fabrication, (b) 2 d, (c) 4 d and (d) 6 d.

Figure 4. Diameter and concentration of BNBs in water. (a) mean and mode diameters. The mean diameter of BNBs was initially about 89 nm and gradually increased to more than two times (about 200 nm). (b) concentration and total volume of BNBs. The concentration of BNBs was initially about 3.47 ± 0.39 ×108 NBs/mL and gradually decreased by 15% (0.61 ± 0.03 × 108 NBs/mL). However, there was almost no change in total volume of NBs after 6 d.

Figure 5. Size distribution of BNBs in water: time evolution of size distribution: (a) just after fabrication and 1 d, (b) 2 d, (c) 4 d and (d) 6 d. The size distribution of BNBs was initially ranged from about 10 to 250 nm and the number of smaller particles decreases, while larger particles grow in size with time (ranged from about 10 to 530 nm after 6 d).

Figure 6. Growth rate of BNBs. The measured cubic radius of NBs linearly increased with time, which is a same trend predicted by the LSW theory for Ostwald ripening.

Figures

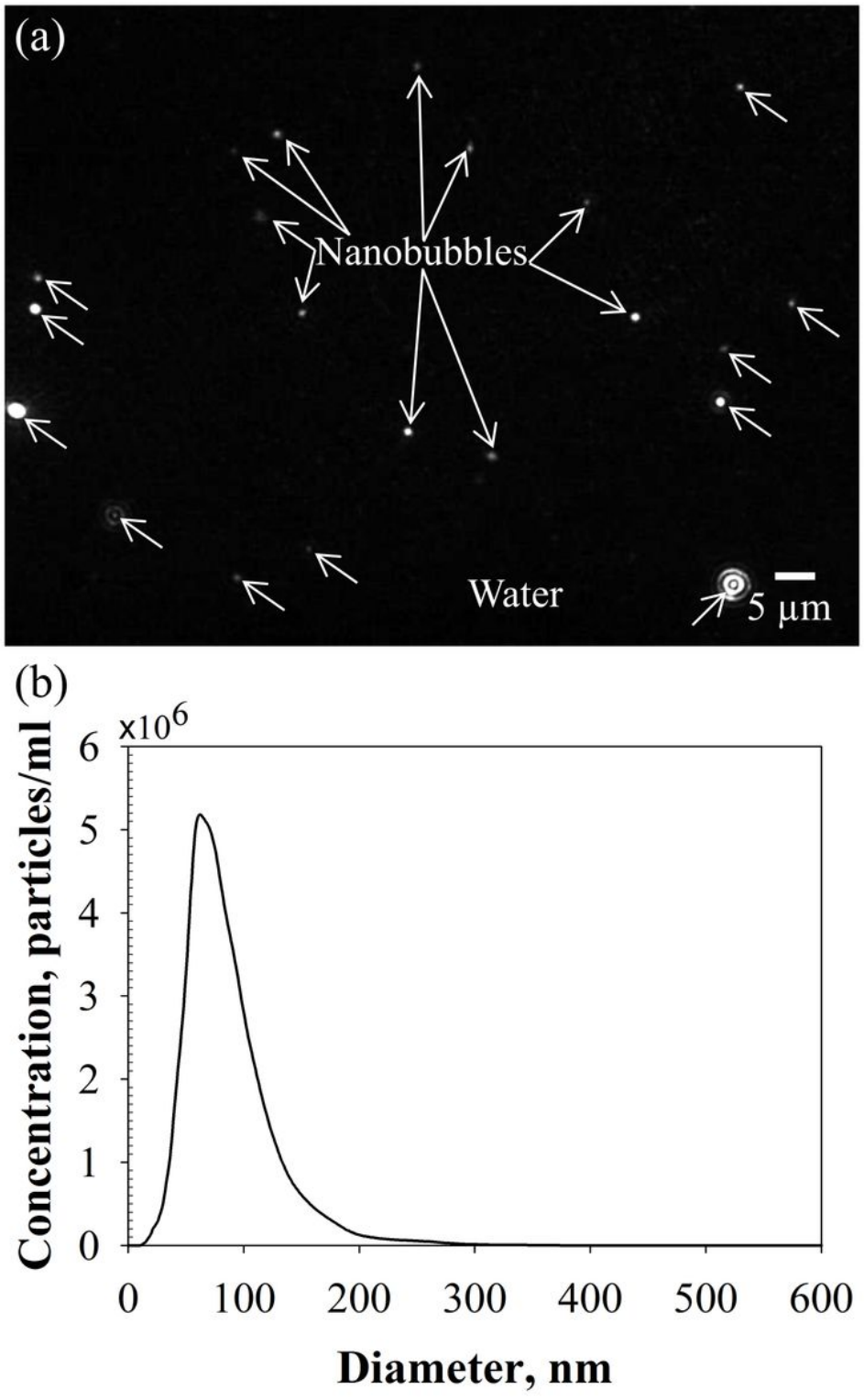

Figure 1

Fabricated BNBs in water. (a) images of BNBs. Black background and white dots represent the water and BNBs, respectively. (b) size distribution of BNBs just after their generation in water.

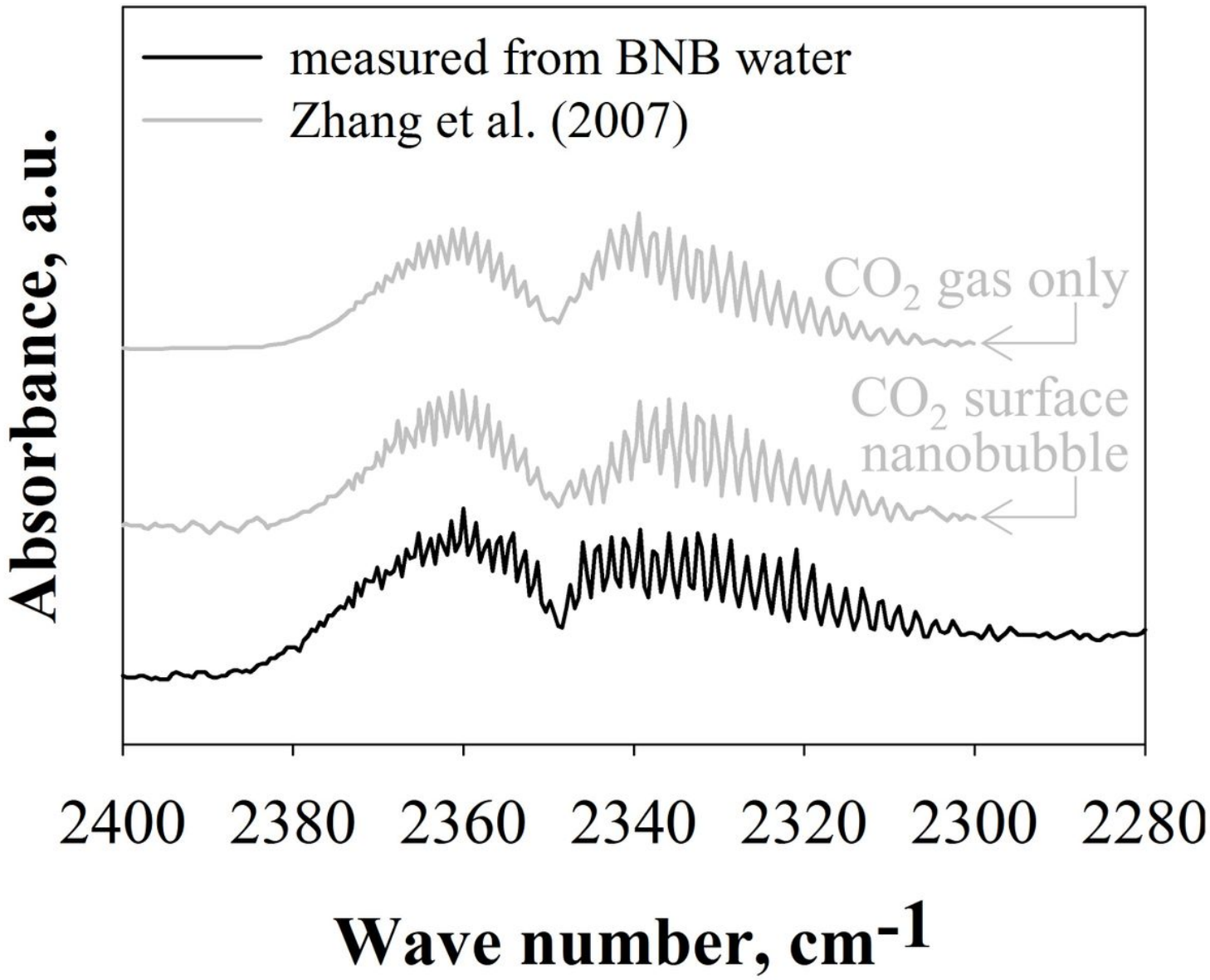

Figure 2

ATR-FTIR spectra of gaseous CO2 in surface nanobubbles and BNBs. The spectrum shows two groups of distinctive fine peaks that were attributed to CO2 gas molecules. The spectrum of BNB water demonstrates the formation of gaseous CO2 bubbles.

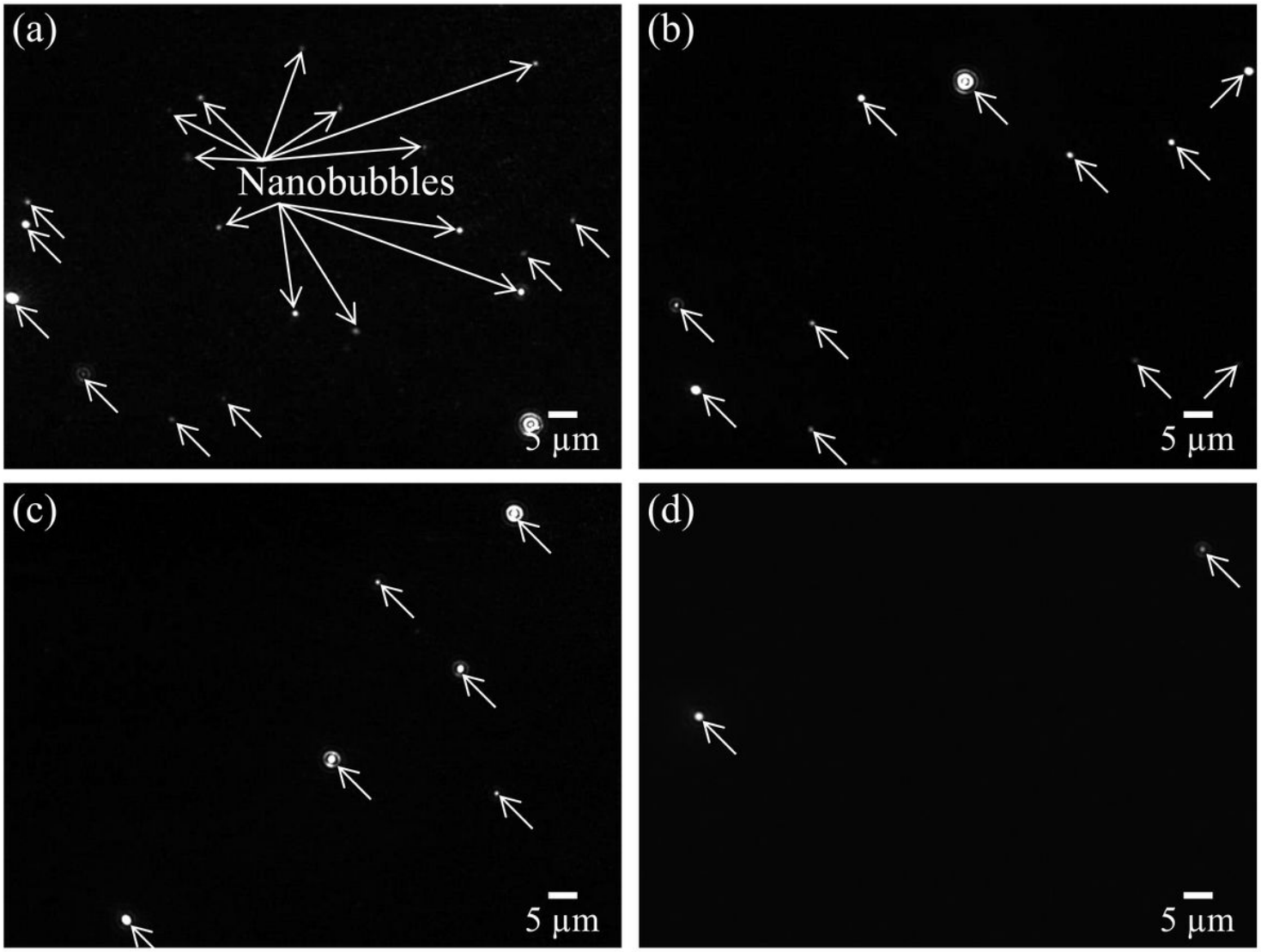

Figure 3

Images of BNBs in water: (a) just after fabrication, (b) 2 d, (c) 4 d and (d) 6 d.

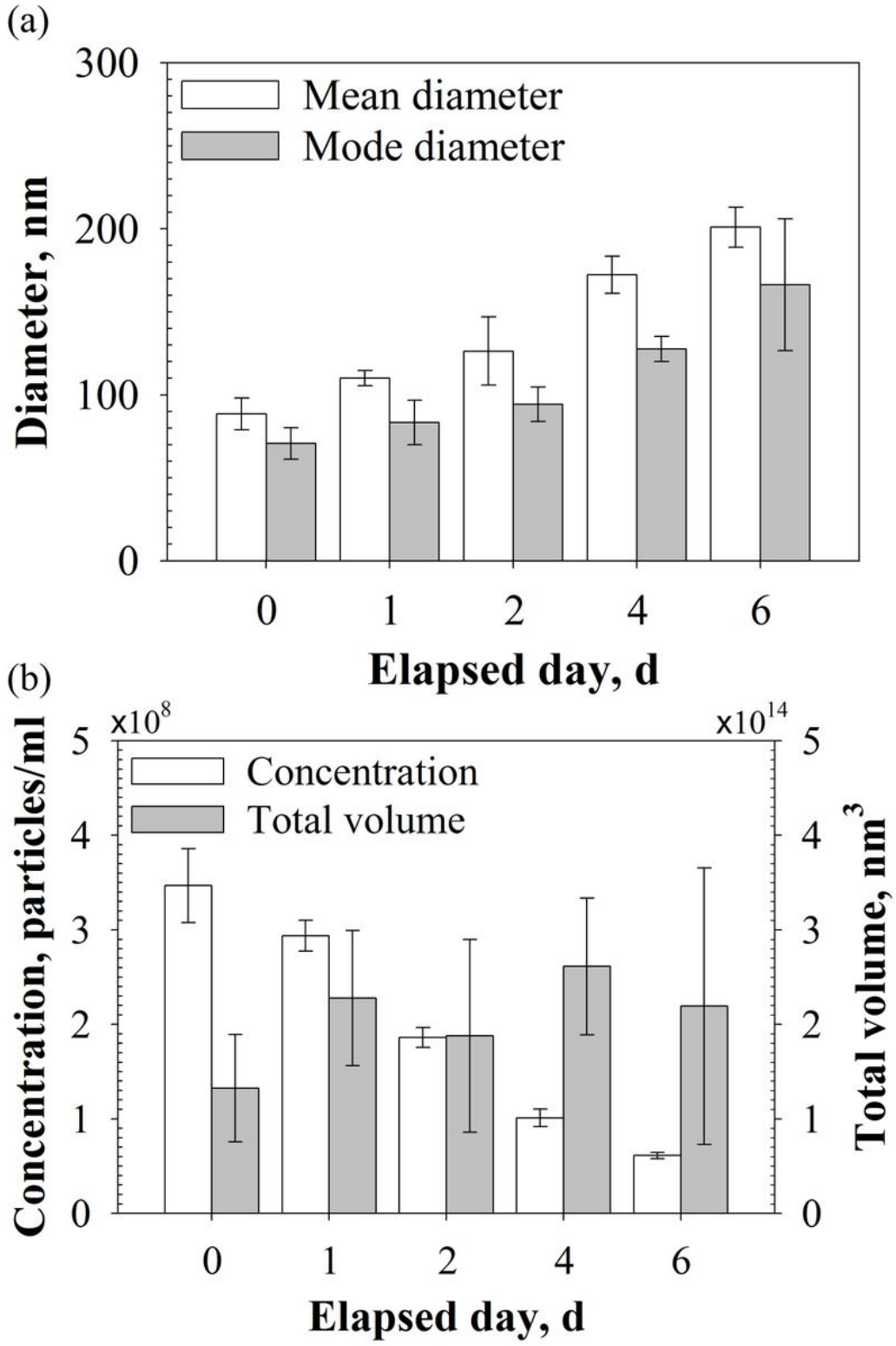

Figure 4

Diameter and concentration of BNBs in water. (a) mean and mode diameters. The mean diameter of BNBs was initially about 89 nm and gradually increased to more than two times (about 200 nm). (b) concentration and total volume of BNBs. The concentration of BNBs was initially about 3.47 ± 0.39 ×108 NBs/mL and gradually decreased by 15% (0.61 ± 0.03 × 108 NBs/mL). However, there was almost no change in total volume of NBs after 6 d.

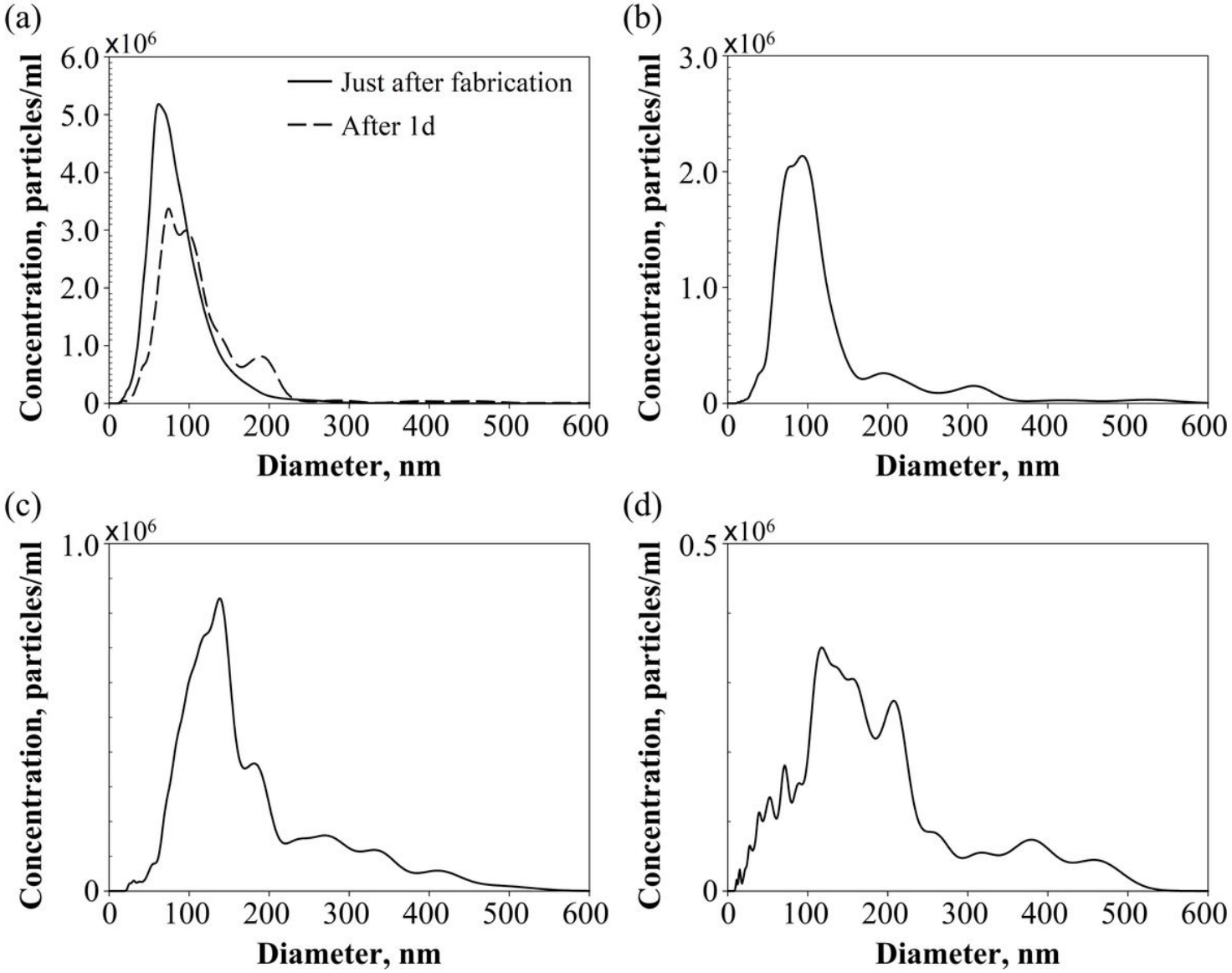

Figure 5

Size distribution of BNBs in water: time evolution of size distribution: (a) just after fabrication and 1 d, (b) 2 d, (c) 4 d and (d) 6 d. The size distribution of BNBs was initially ranged from about 10 to 250 nm and the number of smaller particles decreases, while larger particles grow in size with time (ranged from about 10 to 530 nm after 6 d).

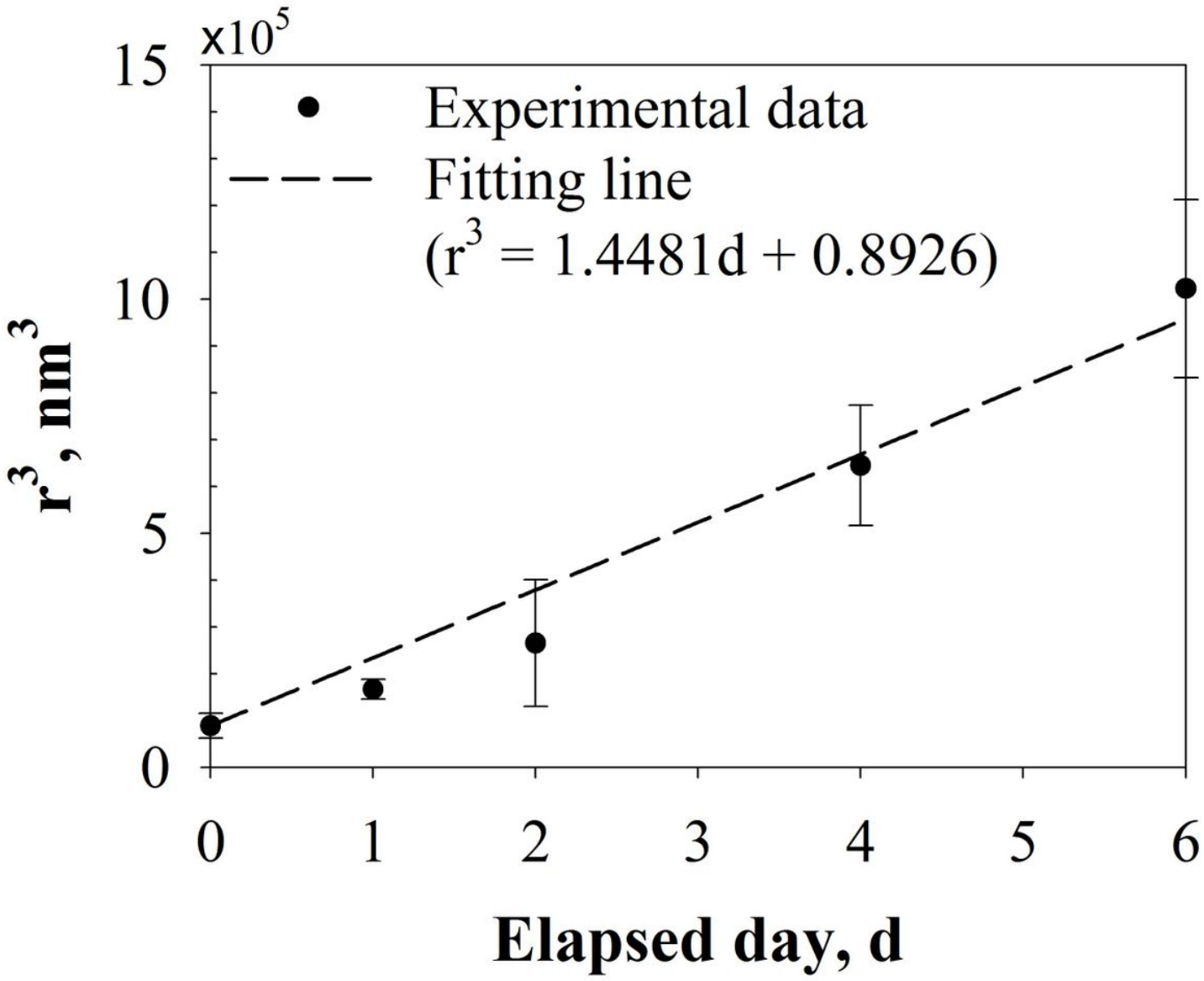

Figure 6

Growth rate of BNBs. The measured cubic radius of NBs linearly increased with time, which is a same trend predicted by the LSW theory for Ostwald ripening.